Inorganic Chemistry Frontiers d2qi01650h

We have presented the Graphical Abstract text and image for your article below. This brief summary of your work will appear in the contents pages of the issue in which your article appears.

1

Tunable thermotropic phase transition triggering large dielectric response and superionic conduction in lead halide perovskites

Dong-Sheng Shao, Lei Sang, Ya-Ru Kong, Zheng-Rong Deng, Hong-Bin Luo,* Zheng-Fang Tian and Xiao-Ming Ren*

Lead halide perovskites show tunable structural phase transition, accompanied by large dielectric response and superionic conduction.

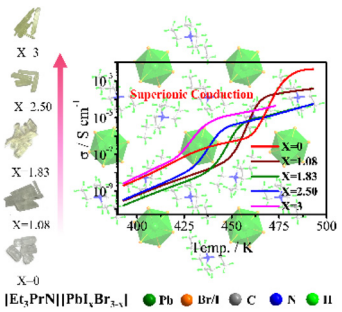

Please check this proof carefully. Our staff will not read it in detail after you have returned it.

Please send your corrections either as a copy of the proof PDF with electronic notes attached or as a list of corrections. **Do not edit the text within the PDF or send a revised manuscript** as we will not be able to apply your corrections. Corrections at this stage should be minor and not involve extensive changes.

Proof corrections must be returned as a single set of corrections, approved by all co-authors. No further corrections can be made after you have submitted your proof corrections as we will publish your article online as soon as possible after they are received.

Please ensure that:

- The spelling and format of all author names and affiliations are checked carefully. You can check how we have identified the authors' first and last names in the researcher information table on the next page. **Names will be indexed and cited as shown on the proof, so these must be correct.**
- Any funding bodies have been acknowledged appropriately and included both in the paper and in the funder information table on the next page.
- All of the editor's queries are answered.
- Any necessary attachments, such as updated images or ESI files, are provided.

Translation errors can occur during conversion to typesetting systems so you need to read the whole proof. In particular please check tables, equations, numerical data, figures and graphics, and references carefully.

Please return your **final** corrections, where possible within **48 hours** of receipt, by e-mail to: InorgChemFrontiersPROD@rsc.org. If you require more time, please notify us by email.

Funding information

Providing accurate funding information will enable us to help you comply with your funders' reporting mandates. Clear acknowledgement of funder support is an important consideration in funding evaluation and can increase your chances of securing funding in the future.

We work closely with Crossref to make your research discoverable through the Funding Data search tool (http://search.crossref.org/funding). Funding Data provides a reliable way to track the impact of the work that funders support. Accurate funder information will also help us (i) identify articles that are mandated to be deposited in **PubMed Central (PMC)** and deposit these on your behalf, and (ii) identify articles funded as part of the **CHORUS** initiative and display the Accepted Manuscript on our web site after an embargo period of 12 months.

Further information can be found on our webpage (http://rsc.li/funding-info).

What we do with funding information

We have combined the information you gave us on submission with the information in your acknowledgements. This will help ensure the funding information is as complete as possible and matches funders listed in the Crossref Funder Registry.

If a funding organisation you included in your acknowledgements or on submission of your article is not currently listed in the registry it will not appear in the table on this page. We can only deposit data if funders are already listed in the Crossref Funder Registry, but we will pass all funding information on to Crossref so that additional funders can be included in future.

Please check your funding information

The table below contains the information we will share with Crossref so that your article can be found *via* the Funding Data search tool. **Please check that the funder names and grant numbers in the table are correct and indicate if any changes are necessary to the Acknowledgements text.**

Funder name	**Funder's main country of origin**	Funder ID (for RSC use only)	**Award/grant number**
Natural Science Foundation of Jiangsu Province	China	501100004608	BK20210543
National Natural Science Foundation of China	China	501100001809	22073047 22101131
Priority Academic Program Development of Jiangsu Higher Education Institutions	China	501100012246	Unassigned

Researcher information

Please check that the researcher information in the table below is correct, including the spelling and formatting of all author names, and that the authors' first, middle and last names have been correctly identified. **Names will be indexed and cited as shown on the proof, so these must be correct.**

If any authors have ORCID or ResearcherID details that are not listed below, please provide these with your proof corrections. Please ensure that the ORCID and ResearcherID details listed below have been assigned to the correct author. Authors should have their own unique ORCID iD and should not use another researcher's, as errors will delay publication.

Please also update your account on our online manuscript submission system to add your ORCID details, which will then be automatically included in all future submissions. See here for step-by-step instructions and more information on author identifiers.

First (given) and middle name(s)	**Last (family) name(s)**	**ResearcherID**	**ORCID iD**
Dong-Sheng	Shao		
Lei	Sang		
Ya-Ru	Kong		
Zheng-Rong	Deng		

Hong-Bin	Luo		0000-0002-2225-7072
Zheng-Fang	Tian		0000-0002-8212-778X
Xiao-Ming	Ren		

Queries for the attention of the authors

Journal: **Inorganic Chemistry Frontiers** Paper: **d2qi01650h**

Title: **Tunable thermotropic phase transition triggering large dielectric response and superionic conduction in lead halide perovskites**

For your information: You can cite this article before you receive notification of the page numbers by using the following format: (authors), Inorg. Chem. Front., (year), DOI: 10.1039/d2qi01650h.

Editor's queries are marked like this Q1, Q2, and for your convenience line numbers are indicated like this 5, 10, 15, ...

Please ensure that all queries are answered when returning your proof corrections so that publication of your article is not delayed.

Query Reference	Query	Remarks
Q1	Please check that the inserted CCDC numbers are correct.	Correct
Q2	Have all of the author names been spelled and formatted correctly? Names will be indexed and cited as shown on the proof, so these must be correct. No late corrections can be made.	Correct
Q3	Please check that the addresses and affiliation links have been displayed correctly.	Correct
Q4	The first line of the Abstract has been inserted as the Graphical Abstract text. Please check that this is suitable. If the text does not fit within the two horizontal lines, please trim the text and/ or the title.	Checked
Q5	The sentence beginning "Solid-solid phase" has been altered for clarity, please check that the meaning is correct.	Correct
Q6	"Robinson" is not cited as an author of ref. 36. Please indicate any changes required.	No changes required.
Q7	The sentence beginning "It failed to" has been altered for clarity, please check that the meaning is correct.	correct
Q8	Please note that a conflicts of interest statement is required for all manuscripts. Please read our policy on conflicts of interest (rsc.li/conflicts) and provide a statement with your proof corrections. If no conflicts exist, please state that "There are no conflicts to declare".	There are no conflicts to declare.
Q9	Have all of the funders of your work been fully and accurately acknowledged? If not, please ensure you make appropriate changes to the Acknowledgements text.	Yes, no changes required.

INORGANIC CHEMISTRY FRONTIERS

RESEARCH ARTICLE

Tunable thermotropic phase transition triggering large dielectric response and superionic conduction in lead halide perovskites†

Cite this: DOI: 10.1039/d2qi01650h

Dong-Sheng Shao,[a] Lei Sang,[a] Ya-Ru Kong,[a] Zheng-Rong Deng,[a] Hong-Bin Luo,[a]* Zheng-Fang Tian[b] and Xiao-Ming Ren*[a,c,d]

Received 30th July 2022,
Accepted 6th September 2022

DOI: 10.1039/d2qi01650h

rsc.li/frontiers-inorganic

Lead halide perovskites have been demonstrated as multifunctional materials. Herein, we demonstrate the tunable thermotropic phase transitions and optical bandgap, together with large dielectric response and superionic conduction through mixed halogen anion modification in a family of bromide-iodide lead halide perovskites $[Et_3PrN][PbI_xBr_{3-x}]$ (Et_3PrN^+ = triethylpropylammonium and x = 0, 1.08, 1.83, 2.50 and 3; labeled as **1–5** sequentially). All members in this family are isomorphic at room temperature, crystallizing in the monoclinic space group $P2_1/n$ or $P2_1/c$, and undergo a phase transition above 440 K. DSC revealed a phase transition that is relevant to the order-to-disorder transformations of globular-shaped cations. Significantly, the lead halide perovskites exhibit superionic conduction beyond 10^{-3} S cm^{-1} in the high-temperature (HT) phase. This study provides an efficient strategy for design of multifunctional lead halide perovskites.

Introduction

Solid-solid phase transitions triggered by external stimuli (*e.g.*, temperature, radiation or stress) have been observed in a range of materials. This type of phase transition frequently associates with massive changes of some physical properties in electrics, optics and magnetism;[1–5] in addition, some solid-solid phase transitions show high latent heat.[6] Consequently, the solid-solid phase transition materials have garnered persistent research interest owing to their vast potential applications in memory devices, sensors, switches, *etc.*[7–9] and thermal energy storage and conversion.[10,11]

Over the past decade, lead halide perovskites have become a versatile platform for realizing phase transition materials. Such types of perovskites, especially three-dimensional (3D) perovskites, generally adopt the molecular formula of ABX_3, wherein A is a monovalent organic cation,[12–15] and B and X are the Pb^{2+} ion and halogen anion, respectively. Typically, in these 3D lead halide perovskites, the Pb^{2+} ions are coordinated by six halogen anions to give PbX_6 octahedra, and the organic cations are accommodated in the interstices between PbX_6 octahedrons. Notably, the organic cations are highly flexible,[16] which may have considerable freedom of motion; as a result, the organic cations often undergo order-to-disorder transformations[17–19] as induced by temperature, thereby leading lead halide perovskites to undergo structural phase transitions. To date, many 3D, 2D and 1D lead halide perovskites with structural phase transitions have been reported[20–26] owing to the diversity of organic cations and variability of concomitant structures; more importantly, phase transition along with the simultaneous physical properties of lead halide perovskites are tunable through structure modification, and it is favorable for design of ideal multifunctional materials. For example, Xiong *et al.*[27] discovered that, by introducing halogen atoms into the organic cations of $[CH_3NH_3]PbI_3$, the phase transition temperature has been tuned in a wide range from 184 to 312 K, and therefore, achieved room-temperature lead iodide perovskite ferroelectrics. Ye and co-workers[28] reported that the phase transitions of lead halide perovskites are tunable through the replacement of halogen anions, and the synthesized lead halide perovskites $[C_4H_{10}NS]PbX_3$ (X = Cl, Br, and I) with different halogen anions display diverse phase transitions and the accompanied band gap, dielectric and second-harmonic generation properties. On the other hand, several studies demonstrated that the tunable band gap is

[a]State Key Laboratory of Materials-Oriented Chemical Engineering and College of Chemistry and Molecular Engineering, Nanjing Tech University, Nanjing 211816, P. R. China. E-mail: hbluo@njtech.edu.cn, xmren@njtech.edu.cn; Tel: +86-25-58139476
[b]Hubei Key Laboratory for Processing and Application of Catalytic Materials, Huanggang Normal University, Huanggang 438000, P. R. China
[c]College of Materials Science and Engineering, Nanjing Tech University, Nanjing 211816, P. R. China
[d]State Key Laboratory of Coordination Chemistry, Nanjing University, Nanjing 210093, P. R. China

† Electronic supplementary information (ESI) available. CCDC 2174163–2174166. For ESI and crystallographic data in CIF or other electronic format see DOI: https://doi.org/10.1039/d2qi01650h

coupled with the photoluminescence of lead halide perovskites with mixed halogen anions.[29–31] However, to the best of our knowledge, it is rarely reported that the tunable phase transitions of lead halide perovskites are achieved through introducing mixed halogen anions, which may be a facile way to manipulate the phase transitions, and endow lead halide perovskites with unprecedented physical properties.

In this work, we present a feasible approach of anion modification by incorporating mixed halogen anions into lead halide perovskites to manipulate the phase transitions as well as the dielectric responses and ionic conduction. We have successfully synthesized a series of bromide-iodide mixed lead halide perovskites $[Et_3PrN][PbI_xBr_{3-x}]$ (x = 0, 1.08, 1.83, 2.50 and 3; labeled as **1–5** sequentially). In the lattice of **1–5**, the globular-shaped quaternary ammoniums easily gain rotational degrees of freedom, leading to order-to-disorder transformation, as expected, and all members in this family undergo a phase transition at a certain temperature, moreover, initiating large dielectric responses and superionic conduction ($\sigma > 10^{-3}$ S cm^{-1}) in the HT phase.

Results and discussion

Crystal structure and halide content

Single-crystal X-ray diffraction analysis revealed that **1** crystallizes in the monoclinic centrosymmetric space group of $P2_1/c$ at 100 K, and is isomorphic to the iodide analogue $[Et_3PrN][PbI_3]$ (**5**)[32] that was previously reported by us. As shown in Fig. 1a, an asymmetric unit of **1** is composed of two crystallographically independent Pb^{2+} ions (Pb1 and Pb2), three different Br^- ions (Br1, Br2 and Br3), and one Et_3PrN^+ cation. Both Pb1 and Pb2 ions are coordinated by six Br^- ions to form a distorted coordination octahedron, in which the Pb–Br bond lengths fall in the range of 3.0046(5)–3.0483(6) Å, and Br–Pb–Br bond angles range from 78.465(13) to 180.0°. The neighboring $PbBr_6$ octahedra are connected through face-sharing mode into a one-dimensional (1D) infinite $\{PbBr_3\}_\infty$ chain along the a-axis. As indicated in Fig. 1c, the Et_3PrN^+ cations fall in the spaces of inter-chains of $\{PbBr_3\}_\infty$.

By partially replacing bromide ions in the lattice of **1** with iodide ions, we have prepared a series of mixed-halide perovskites $[Et_3PrN][PbI_xBr_{3-x}]$ (**2**, x = 1.08; **3**, x = 1.83; **4**, x = 2.50). Single crystal structure refinements demonstrate that the Br^- and I^- ions are randomly distributed at the halide sites to give the mixed-halide inorganic $\{PbI_xBr_{3-x}\}_\infty$ chain, and the molar ratio of Br/I was determined according to their site-occupancy factors, to give 1.08 (**2**), 1.83 (**3**) and 2.50 (**4**), respectively. As shown in Fig. S1,† all powder X-ray diffraction (PXRD) patterns of mixed-halide perovskites match well with the simulated patterns obtained from their single crystal structures, indicating that the obtained mixed-halide perovskites possess high phase purity. The elemental microanalyses for C, H and N together with energy dispersive spectroscopy (EDS) for Br and I have been performed for the mixed-halide perovskites and the results are collected in Table 1, indicating that the molar fractions (x) in **2–4** acquired from different techniques are consistent with each other.

PXRD patterns of isomorphic **1–5** display high similarity (Fig. 2a); however, most of the diffraction positions shift gradually toward smaller angles in this family with increasing the molar fraction of I^- ions (Fig. 2b). This observation indicates that I^- ions substituting Br^- ions lead to some inter-planar spacing expansion owing to the ionic radius of iodide being larger than that of bromide.[33] Interestingly, the cell parameters show non-monotonic changes with the molar fraction (x) of I^- ions in **1–5**. As shown in Fig. 2c, the lengths of the a- and b-axis and V increase with x increasing, whereas the length of

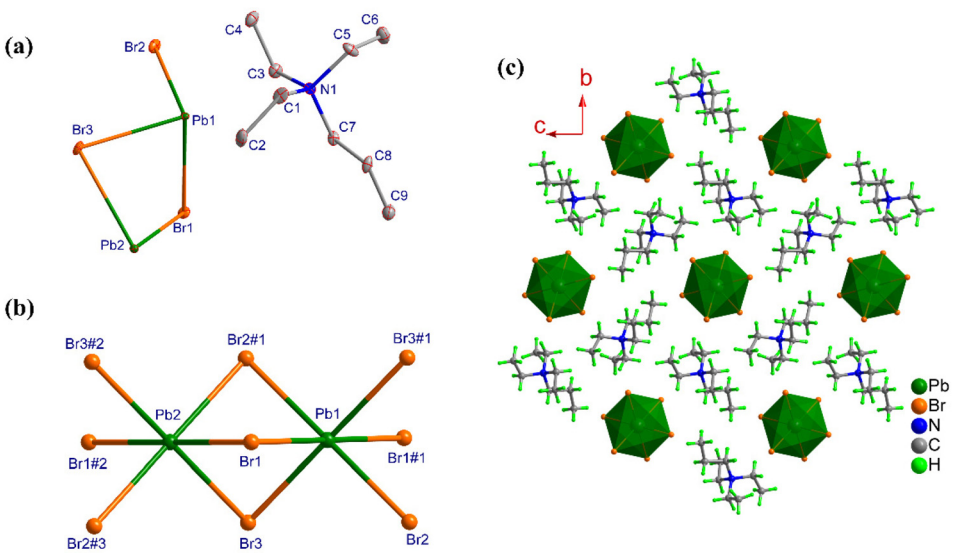

Fig. 1 (a) Asymmetric unit in **1** with thermal ellipsoids drawn at the 50% probability level. (b) Two types of $PbBr_6$ octahedra in **1** with the symmetric codes #1 = 1 − x, −y, 1 − z; #2 = 2 − x, −y, 1 − z; #3 = 1 + x, y, z. (c) Packing diagram of **1** viewed along the a-axis.

Table 1 The molar fraction (x) determined by crystal structure refinement, EDS and elemental analyses in **2–4**

	Crystal	EDS/Atom%			Elemental analysis			
Compound	x	Br%	I%	x	C%	H%	N%	x
2	1.08	11.52	6.01	1.03	16.83	3.45	2.18	1.09
3	1.83	6.00	8.82	1.79	15.97	3.28	1.82	1.85
4	2.50	3.03	13.25	2.44	15.32	3.20	1.75	2.45

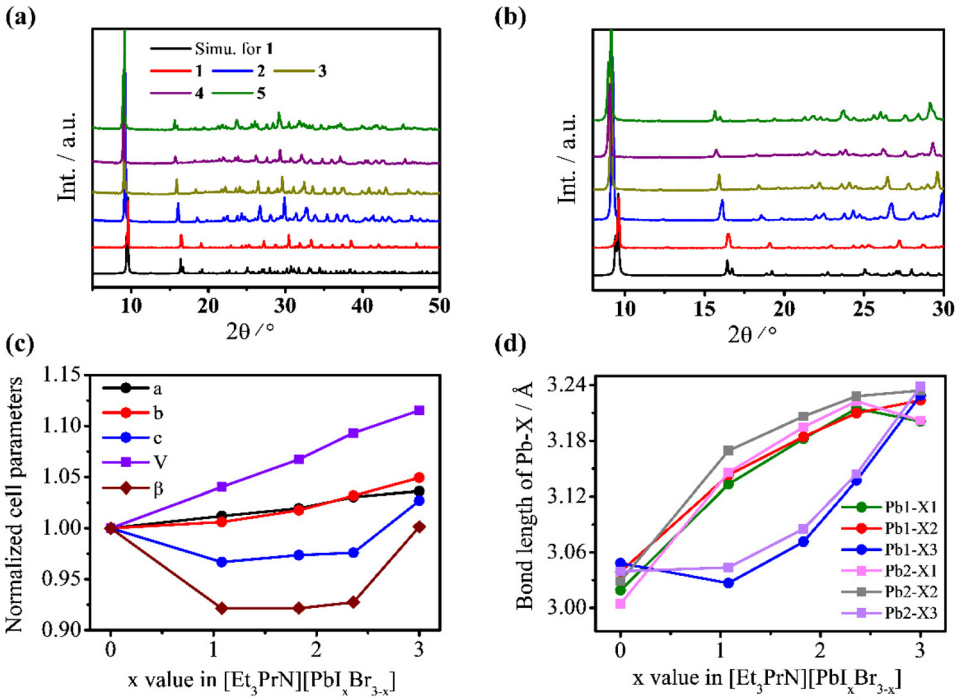

Fig. 2 (a and b) PXRD patterns of **1–5**. Plots of (c) unit cell parameters *versus* the molar fraction (x) and (d) Pb–Br/I bond length in **1–5**.

the c-axis and β angle in **2–4** shrink for the two parent perovskites **1** and **5**.

The Pb–X (X = Br or I) bond lengths and the distorted degree of the PbX_6 octahedron in **1–5** are inspected, and the results are depicted in Fig. 2d and summarized in Table 2, respectively. In general, the octahedral distortion of PbX_6 can be estimated using the parameter of Δ_{oct} through eqn (1),[34,35]

$$\Delta_{oct} = \frac{1}{6}\sum_{i=1}^{6}[(d_i - d_m)/d_m]^2 \quad (1)$$

In eqn (1), d_m and d_i represent the mean Pb–X bond distance and six individual Pb–X bond distances, respectively. In addition, Robinson *et al.*[36] developed another method to quantitatively evaluate a PbX_6 octahedron distortion, in which the distortion parameters concern the bond angle (bite angle) variance, σ^2_{oct}, with the expression below,

$$\sigma^2_{oct} = \frac{1}{11}\sum_{i=1}^{12}(\alpha_i - 90)^2 \quad (2)$$

Table 2 Distortion parameters for PbX_6 octahedra in **1–5**

Compound	**1**		**2**		**3**		**4**		**5**	
Octahedron	Pb1	Pb2	Pb1	Pb2	Pb1	Pb2	Pb1	Pb2	Pb1	Pb2
d_m/Å	3.035	3.024	3.101	3.120	3.147	3.162	3.187	3.198	3.218	3.225
$\Delta_{oct} \times 10^{-5}$	1.613	2.331	28.87	30.54	29.18	29.72	12.88	14.30	1.457	2.545
σ^2_{oct}	43.62	38.63	25.52	32.54	21.63	26.66	21.57	25.24	20.56	22.85

In eqn (2), α_i represents the X–Pb–X angle adopting cis-arrangement of two X^- ions in a PbX_6 octahedron. The results in Table 2 display that there are smaller differences for the parameters d_m and Δ_{oct} in the two parent compounds **1** and **5**, while bigger differences are observed in the three mixed-halide perovskites **2–4** for both the average Pb–X bond length (d_m) and the distorted parameter (Δ_{oct}) between two inequivalent PbX_6 octahedra, and this distinction is due to I^- and Br^- ions having distinct radii. The distorted parameter (σ^2_{oct}), which concerns that the bite angles deviate from a right angle in a PbX_6 coordination octahedron, decreases with the molar fraction (x) of I^- ions increasing. In addition, two different PbX_6 coordination octahedra show a much distinct distortion parameter σ^2_{oct} in **1–5**.

Phase transition behavior

Differential Scanning Calorimetry (DSC) plots, with two sequential heating and cooling runs, are displayed in Fig. 3a and Fig. S3† for **1–5**. A couple of endothermic and exothermic peaks are clearly observed at 480/470 K in the first heating-cooling run in the DSC plot of **1**, suggesting that, therein, a reversible phase transition occurs. As for **2–5**, the reversible thermotropic phase transition temperature is around 470/458 K (**2**), 461/451 K (**3**), 452/443 K (**4**) and 445/440 K (**5**) (Fig. S3a–3d), respectively. The two parent compounds **1** and **5** exhibit the highest and the lowest temperature of phase transition (480/470 K for **1**, Fig. 3a; 445/440 K for **5**, Fig. S3d†), and the phase transition temperatures in **2–4** fall within the interval of those in **1** and **5**, and moreover, show a decreasing trend with the increasing molar fraction (x) of I^- ions. The endothermic or exothermic anomaly peaks in the second heating-cooling run shift slightly toward lower temperature with respect to those in the first heating-cooling process because the dynamic motion of alkyl chains in Et_3PrN^+ cations is unable to follow the quick change of temperature during the DSC measurement, and the similar phenomena have been universally observed in the ion-liquid crystals.[37,38]

The phase transition enthalpy changes (ΔH) in the first heating process are estimated to be 20.9 kJ mol^{-1} (**1**), 14.96 kJ mol^{-1} (**2**), 14.18 kJ mol^{-1} (**3**) and 13.14 kJ mol^{-1} (**4**), respectively. The ΔH values in mixed-halide perovskites are comparable to that in **5** (14.40 kJ mol^{-1}), while less than that in **1**. The phase transition entropy changes (ΔS) have been calculated by the equation $\Delta S = \Delta H/T_c$ to be 43.54, 31.83, 30.76, 29.70 and 32.36 J mol^{-1} K^{-1} for **1–5** in sequence; herein, ΔH and T_c are the phase transition enthalpy changes and critical temperature, respectively. The phase transition ΔS may be expressed as $\Delta S = R \ln N$ in statistical thermodynamics, in which R and N represent the gas constant and the ratio of state numbers of possible configurations between HT and low-temperature (LT) phases. The N values are gauged to be 188 (**1**), 46 (**2**), 40 (**3**), 33 (**4**) and 49 (**5**), and such large N values suggest that the phase transition in **1–5** arises from the order–disorder structural transformation, which is probably relevant to the order-to-disorder transformation of alkyl chains in cations. Notably, the large ΔS values suggest that **1–5** might be promising barocaloric materials,[39,40] and the large phase transition entropy is attributed to the heavily disordered alkyl chains of tetraalkylammonium cations, which is also observed in other hybrid perovskites.[39,40]

Plots of dielectric permittivity (ε') *versus* temperature at the selected frequencies are shown in Fig. 3b and Fig. S5† for **1–5**. All compounds show a dielectric phase transition in the vicinity of the thermal anomaly, with the peak temperature of 478 K (**1**), 463 K (**2**), 453 K (**3**), 443 K (**4**) and 432 K (**5**) in the curve of ε' *vs.* T. These peak temperatures are slightly lower than that acquired from DSC measurements because the temperature change rates are distinct for the two techniques. **1–5** exhibit a comparable change tendency of ε' against T; herein, the changes of ε' *versus* T in **1** are described in detail. The ε' value of **1** is independent of temperature and frequency in 200–432 K, suggesting that the thermally activated dipole motion is suppressed below 432 K, and strongly related to the frequency above 432 K, and followed with a dielectric permittivity peak. The dielectric permittivity, related to the dipole motion or ion displacement,[41,42] is closely dependent on the crystal structure of a material, and the large dielectric anomaly in **1–5** is possible to arise from the order-disorder transformation of alkyl chains in cations or the relative displacement of cations to inorganic $\{PbX_3\}_\infty$ chains. The change of an alkyl

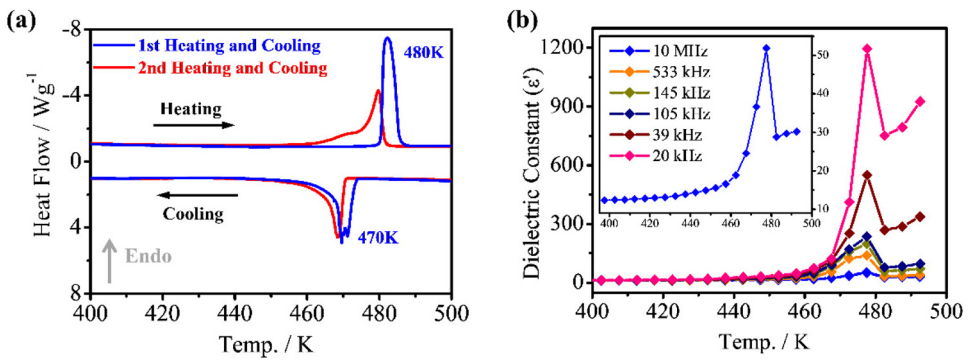

Fig. 3 (a) DSC curves with two sequential heating-cooling runs, and (b) temperature dependence of the dielectric permittivity (ε') at selected frequencies for **1** (the inset figure shows the magnified dielectric permittivity at 10 MHz).

chain conformation does not significantly alter its dipole, and therefore, the large variation of dielectric permittivity around transition temperature arises from the ion displacement in the lattice.

It failed to determine the crystal structures of **1–5** in the HT phase owing to cations being highly disordered, making it impossible to define the atomic sites in cations. Alternatively, the variable-temperature PXRD technique was used for inspection of structure changes between LT and HT phases, and variable-temperature PXRD patterns are displayed in Fig. 4 and Fig. S4† for **1–5**. The five compounds display similar trends of PXRD patterns changing with temperature from LT to HT phases, and herein, only variable-temperature PXRD patterns of **1** are analyzed in detail. At first glance all PXRD patterns of **1** in 303–493 K show high similarity, implying that the crystal structures are quite analogous to each other in both LT and HT phases (*e.g.*, PXRD patterns at 443, 473 K in LT phase and at 483, 493 K in HT phase). However, the imperceptible changes are also obvious when PXRD patterns are carefully compared to each other. With rising temperature in 303–493 K, some diffraction peaks start to split into two or three peaks; for example, the broad and asymmetric peak with 2θ = 9.20° at 303 K corresponding to the overlap of (020) and (011) diffractions shifts toward the smaller 2θ angle side with increasing temperature, and splits into two peaks from 323 to 493 K (Fig. 3b), and the diffraction peaks with 2θ = 15.82° and 18.67° at 303 K originating from (120) and (130) diffractions show a similar variation tendency as temperature increases. It is worth noting that, with temperature further elevated above 493 K, the several split peaks in 303–493 K combine together into a single peak again, and the main diffractions of (020), (011), (013), (120), (130), (140) and (220) remain; moreover, all diffractions shift to the smaller 2θ angle side. The diffraction peak splitting in 303–493 K is probably due to the changes of cell parameters with the increasing temperature. As temperature increases above 493 K, many of the diffraction peaks in the PXRD patterns show very low intensity, and only several peaks are distinctly observed. This is because the globular-shaped cations gain more thermal energy at high temperature, and the rotational freedom degrees of cations are much increased, leading to plastic crystal behavior.[43,49] Actually, the crystals of **1** show plastic deformation in the HT phase (Fig. S6†). On the basis of the above analysis, the phase transitions occurred in **1–5** are mainly ascribed to the order–disorder transformation of the alkyl chain conformation in cations.

Changes of color and optical bandgap

UV-visible absorption spectra of **1–5** in Fig. 5b show the tunable onset of the absorption band, and the onset of the absorption band moves from the wavelength of 353.9 nm to 421.9 nm as the molar fraction (x) of I^- ions increases, leading to the color of **1–5** changing from colorless to yellow in sequence (Fig. 5a). The electron band structures were calculated for **1** and **5** (Fig. S7†), respectively, revealing that both **1** and **5** are indirect bandgap semiconductors, and thus, the Kubelka–Munk plot is obtained from the absorption spectrum by the Tauc equation eqn (3),[44] in which $F(R_\infty)$ is the Kubelka–Munk function[45] and A is a constant. The Kubelka–Munk plot is displayed in Fig. 5c.

$$(h\nu \cdot F(R_\infty))^{1/2} = A(h\nu - E_g) \quad (3)$$

The optical band gaps (E_g) of **1–5** are estimated from the Kubelka–Munk plot (Fig. 5c) and depicted in Fig. 5d; the E_g is 3.50 eV for **1**, 3.14 eV for **2**, 3.01 eV for **3**, ~~and~~ 2.95 eV and 2.93 eV for **4** and **5**, respectively, showing a decreasing trend with increasing the molar fraction (x) of I^- ions.

Impedances and conduction

The alternating current (AC) impedance spectra are depicted in Fig. 6a–c and Fig. S8–S12† for **1–5**. The linear Nyquist plots appear at temperatures below 400 K, suggesting the negligible conduction of **1–5**. As the temperature is increased above 400 K, an imperfect arc occurs in each Nyquist plot in the high-frequency region, corresponding to electron/ion transfer in the bulk phase and grain boundary, together with a spur in the low-frequency regime which is relevant to the mobile ions blocked by the electrode/electrolyte interface. **1–5** show typical thermally activated conduction. The Nyquist plots were fitted using the Zview program to give resistances (R) (Fig. S13†), and the ionic conductivity (σ) was calculated according to the equation of $\sigma = L/RS$, where the symbols L and S represent the thickness and cross-sectional area of the compressed pellet

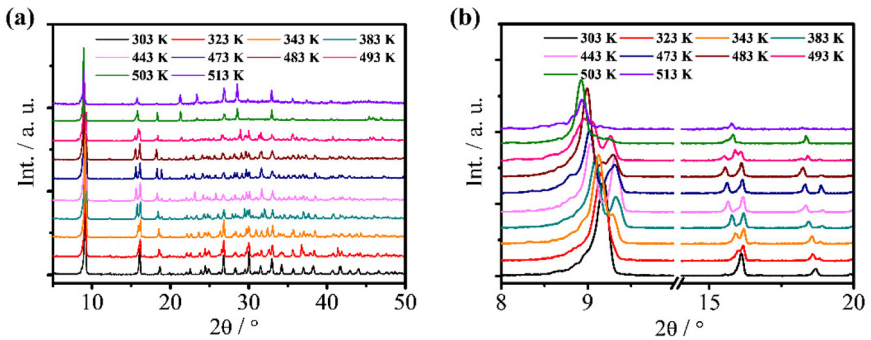

Fig. 4 Variable-temperature PXRD patterns of **1** in the 2θ range of (a) 5–50° and (b) 8–20°.

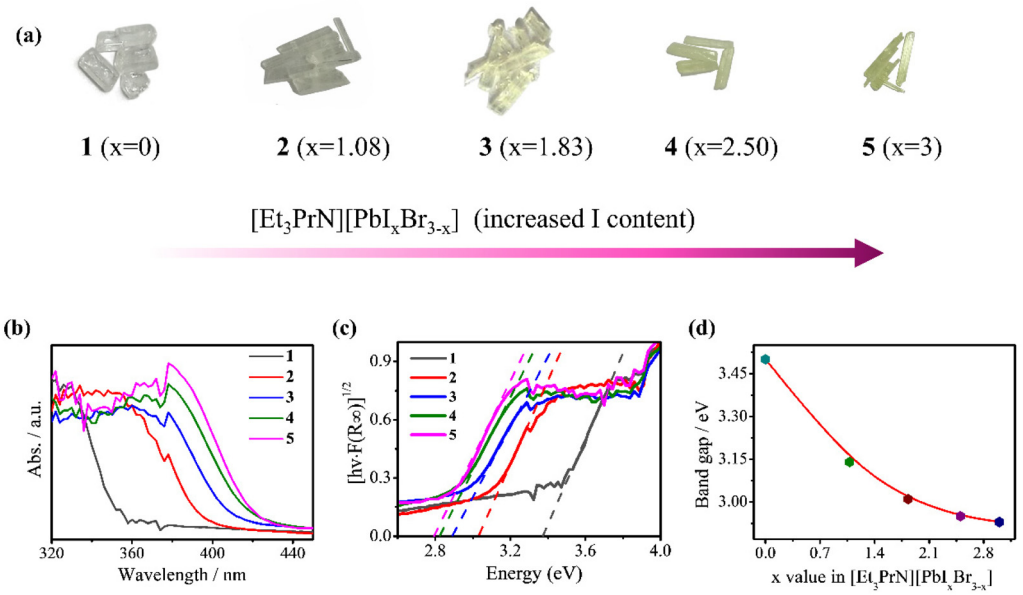

Fig. 5 (a) Photographs of the bulk crystals, (b) UV-visible absorption spectra, (c) Tauc plots and (d) the corresponding calculated E_g values of **1–5**.

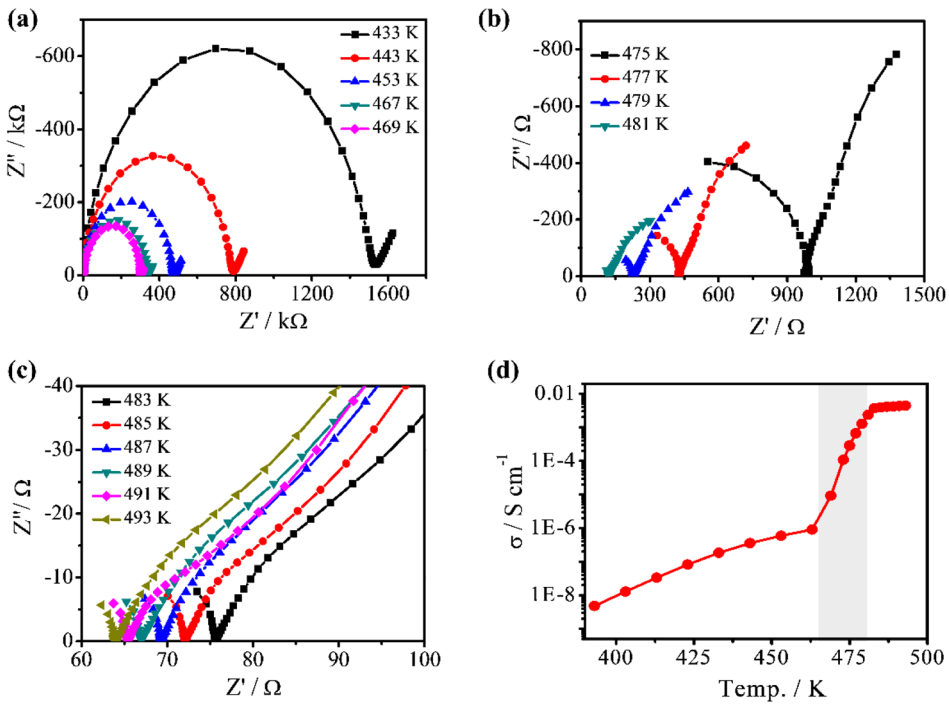

Fig. 6 (a–c) Nyquist plots at selected temperatures and (d) temperature-dependent ionic conductivity of **1**.

sample. The temperature-dependent ionic conductivities are denoted in Fig. 6d for **1** and in Fig. S14† for **2–5**, respectively. **1–5** show rather low conduction ($\sigma = 10^{-10}$–10^{-8} S cm^{-1}) below 400 K owing to the migration of ions being restricted in the lattice, and the σ value increases from 4.75×10^{-9} S cm^{-1} at 393 K to 1.83×10^{-7} S cm^{-1} at 433 K and 9.25×10^{-6} S cm^{-1} at 469 K in **1**. As temperature is increased from 469 K to 479 K, the σ value in **1** is almost improved by three orders of magnitude, with $\sigma = 1.26 \times 10^{-3}$ S cm^{-1} at 479 K, indicating that **1** achieves a superior ionic state above 479 K owing to superionic phase transition.[46–48] The temperature of superionic phase transition coincides with that of the structural phase transition, demonstrating that the superionic phase transition of **1** arises from the structural phase transition. To date, order-to-disorder structural phase transition resulting in sharply increased ionic conductivity is observed in many ionic

conductors.[41,47] In the case of **1**, the orientation and displacement motion of the disordered cations in the lattice provides a facile manner for the ion migration, thereby leading to high ionic conductivity. To further demonstrate that the high conductivity of **1** is mainly contributed by the ionic rather than the electronic conduction, the chronoamperometry measurements were carried out for evaluating the electronic conductivity of **1** (Fig. S15†). It is worth noting that the electronic conductivity of **1** only reaches 2.07×10^{-8} S cm^{-1} even at 463 K, several orders of magnitude less than the total conductivity acquired from AC impedance measurements, unraveling that the ionic conduction dominates in the charge transport process of **1**. As expected, the σ value of **2–5** also sharply jumps around the phase transition temperature; that is, the σ value of **2** increases by three orders of magnitude from 1.03×10^{-7} S cm^{-1} at 453 K to 1.28×10^{-4} S cm^{-1} at 463 K, and the σ is enhanced by two orders of magnitude around the structural phase temperature for **2–5**, to reach the value of 5.55×10^{-6} S cm^{-1} at 453 K, 2.49×10^{-6} S cm^{-1} at 443 K and 3.13×10^{-6} S cm^{-1} at 433 K, respectively. Compared with **2–5**, **1** exhibits higher ionic conduction, especially the superionic conduction ($\sigma > 10^{-3}$ S cm^{-1}) in the HT phase. As mentioned in DSC analysis, **1** displays the largest ratio of state numbers in **1–5**, which is more than 4 times higher than that of **2–5**, suggesting that the cations of **1** in the HT phase acquired much more rotational degrees of freedom and are easy to diffuse and migrate, and this superionic conduction mechanism is similar to the well-known one in organic ionic plastic crystals.[49–51]

Conclusion

In this study, we present the investigations of crystal structure, phase transition, electronic spectra, dielectrics and conduction for a family of mixed lead halide perovskites $[Et_3PrN][PbI_xBr_{3-x}]$ ($0 \le x \le 3$), and demonstrate that the phase transition temperature, optical bandgap and color, and conduction are mediated by the change of x value in $[Et_3PrN][PbI_xBr_{3-x}]$ ($0 \le x \le 3$). Five isomorphic lead halide perovskites show a phase transition at a certain temperature, and in the HT phase, the globular-shaped quaternary ammoniums gain enough rotational degrees of freedom, featuring plastic crystals and leading to a larger enthalpy change of phase transition, large dielectric response and superionic conduction with ionic conductivity beyond 10^{-3} S cm^{-1}. These perovskites might be promising barocaloric, dielectric and ionic conducting materials that can be utilized in various devices. This study discloses that the superionic conducting lead halide perovskite phase transition materials may be achieved by rational molecule design.

Experimental section

Chemicals and materials

All of the chemicals and solvents were purchased from commercial suppliers and used without further purification. Triethylpropylammonium iodide ($[Et_3PrN]I$) and triethylpropylammonium bromide ($[Et_3PrN]Br$) were prepared following a modified procedure that was used for preparation of benzylpyridinium iodide or bromide.[52]

Preparation of $[Et_3PrN][PbBr_3]$ (1)

$PbBr_2$ (1.101 g, 3 mmol) and $[Et_3PrN]Br$ (0.6725 g, 3 mmol) were dissolved in DMF (25 mL) to form a clear colorless solution at ambient temperature. Colorless block-shaped crystals were grown by slow evaporation of the clear colorless solution in an oven at 40 °C for two weeks. The crystals were collected by suction, washed with a little amount of DMF (<1 mL) one time and ethanol three times (3 × 5 mL) sequentially, and dried in air. Yield: ~40%. Anal. calc. for $C_9H_{22}NPb\ Br_3$: C, 18.28; H, 3.75; N, 2.37%. Found: C, 18.27; H, 3.71; N, 2.28%.

Preparation of mixed lead halide perovskites 2, 3, and 4

These mixed-halide crystals were harvested using an analogous process which is described below. A certain molar ratio of $[Et_3PrN]Br$, $[Et_3PrN]I$, $PbBr_2$ and PbI_2 were mixed in a small amount of DMF to prepare a clear solution at ambient temperature, $[Et_3PrN]Br/[Et_3PrN]I/PbBr_2/PbI_2$ = 0 : 1 : 1 : 0 for **2**, 1 : 1 : 1 : 1 for **3** and 1 : 0 : 0 : 1 for **4**, respectively. Afterward, the beaker containing the abovementioned solution was placed in an oven at 40 °C, and the crystals were grown two weeks later, which were collected by suction, washed repeatedly with a small amount of DMF (<1 mL) one time and then ethanol three times (3 × 5 mL), and finally dried in air. Yield: ~66% calculated on the reactant $PbBr_2$ for **2**, ~56% calculated on the reactant $PbBr_2$ for **3**, and ~70% calculated on the reactant PbI_2 for **4**.

Characterization

Elemental analyses (C, H, and N) were performed with an Elementar Vario EL. EDS was carried out by means of a Hitachi S-3400N scanning electron microscope. DSC measurements were performed on a NETZSCH DSC 204F1 Phoenix with a temperature change rate of 10 K min^{-1}. Thermogravimetric analysis (TGA) was performed with an SDT Q600 thermogravimetric analyzer in 300–950 K under a nitrogen atmosphere with a heating rate of 20 K min^{-1}. PXRD data were collected on a Bruker D8 Advance powder diffractometer at ambient temperature, and the measurement was performed at 40 kV and 40 mA, and using Cu Kα radiation (λ = 1.5418 Å). Variable-temperature PXRD measurements were carried out using a SHIMADZU XRD-6100 diffractometer with Cu Kα radiation (λ = 1.5418 Å), operated at 40 kV and 40 mA. Solid-state UV-vis absorption spectra were recorded on a PerkinElmer Lambda 950 UV-vis-near-IR spectrophotometer at ambient temperature.

Dielectric permittivity and impedance spectra were recorded using a Concept 80 system (Novocontrol, Germany) in 123–493K, and the frequencies span from 1 to 10^7 Hz. All of the samples were prepared in the form of a disk with a diameter of 7 mm, and a thickness of *ca.* 0.660 mm, 0.959 mm, 1.003 mm and 1.235 mm for **1–4** sequentially.

X-ray crystallography

Single-crystal X-ray diffraction data were collected for **1–4** at 100 K using the graphite-monochromated Mo Kα (λ = 0.71073 Å) radiation on a CCD area detector (Bruker SMART). Data reduction and absorption corrections were performed with the SAINT[53] and SADABS[54] software packages, respectively. Structures were solved by direct methods using the SHELXL-2014 software package.[55] The non-hydrogen atoms were anisotropically refined using a full-matrix least-squares method on F^2. All hydrogen atoms were placed at the calculated positions and refined as riding on the parent atoms. The details of data collection, structure refinement and crystallography are summarized in Table S1.†

Conflicts of interest

Q8 ■■■■

Acknowledgements

This work was financially supported by Priority Academic Program Development of Jiangsu Higher Education Institutions, National Natural Science Foundation of China (Grant No. 22073047 and 22101131), and Natural Science Q9 Foundation of Jiangsu Province (Grant No. BK20210543).

References

1 M. Hughs, M. Jimenez, S. Khan and M. A. Garcia-Garibay, Synthesis, Rotational Dynamics, and Photophysical Characterization of a Crystalline Linearly Conjugated Phenyleneethynylene Molecular Dirotor, *J. Org. Chem.*, 2013, **78**, 5293–5302.

2 Q. Ye, T. Akutagawa, S. I. Noro, T. Nakamura and R. G. Xiong, Polymorphism and Magnetism of (cis-cyclohexane-1,4-diammonium)(dicyclohexano[18]crown-6)$_2$[Ni(dmit)$_2$]$_2$ Salts, *Cryst. Growth Des.*, 2010, **10**, 4856–4860.

3 W. H. Ning, L. Zhai, J. L. Liu, X. M. Ren, K. Ichihashi, S. Nishihara and K. Inoue, Multiple Structural Transformations Coupled with Switchable Magnetic and Dielectric Responses in an Amphidynamic Crystal of 4′-Tert-butylbenzyl- pyridinium Bis (maleonitriledithiolate) nickelate, *J. Mater. Chem. C*, 2015, **3**, 7906–7915.

4 M. M. Hua, L. Ye, Q. W. Wang, J. J. Ma, Z. X. Gong, Q. Xu, C. Shi and Y. Zhang, A Layered Hybrid Rare-Earth Double-Perovskite-Type Molecule-Based Compound with Electrical and Optical Response Properties, *J. Mater. Chem. C*, 2020, **8**, 16349–16353.

5 C. F. Wang, H. Li, M. G. Li, Y. Cui, X. Song, Q. W. Wang, J. Y. Jiang, M. M. Hua, Q. Xu, K. Zhao, H. Y. Ye and Y. Zhang, Centimeter-Sized Single Crystals of Two-Dimensional Hybrid Iodide Double Perovskite (4,4-Difluoro- piperidinium)$_4$AgBiI$_8$ for High-Temperature Ferroelectricity and Efficient X-Ray Detection, *Adv. Funct. Mater.*, 2021, **31**, 2009457–2009464.

6 P. Xi, F. L. Zhao, P. Fu, X. Q. Wang and B. W. Cheng, Synthesis, Characterization, and Thermal Energy Storage Properties of A Novel Thermoplastic Polyurethane Phase Change Material, *Mater. Lett.*, 2014, **121**, 15–18.

7 G. K. Long, R. Sabatini, M. I. Saidaminov, G. Lakhwani, A. Rasmita, X. G. Liu, E. H. Sargent and W. B. Gao, Chiral-Perovskite Optoelectronics, *Nat. Rev. Mater.*, 2020, **5**, 423.

8 G. F. Nataf, M. Guennou, J. M. Gregg, D. Meier, J. Hlinka, E. K. H. Salje and J. Kreisel, Domain-Wall Engineering and Topological Defects in Ferroelectric and Ferroelastic Materials, *Nat. Rev. Phys.*, 2020, **2**, 634.

9 L. W. Martin and A. M. Rappe, Thin-Film Ferroelectric Materials and Their Applications, *Nat. Rev. Mater.*, 2017, **2**, 16087.

10 H. j. Zhu, D. R. MacFarlane, J. M. Pringle and M. Forsyth, Organic Ionic Plastic Crystals as Solid-State Electrolytes, *Trends Chem.*, 2019, **1**, 126–140.

11 L. He, Y. T. Liu, P. P. Shi, H. L. Cai, D. W. Fu and Q. Ye, Energy Harvesting and Pd(II) Sorption Based on Organic–Inorganic Hybrid Perovskites, *ACS Appl. Mater. Interfaces*, 2020, **12**(48), 53799–53806.

12 W. Li, Z. Wang, F. Deschler, S. Gao, R. H. Friend and A. K. Cheetham, Chemically Diverse and Multifunctional Hybrid Organic–Inorganic Perovskites, *Nat. Rev. Mater.*, 2017, **2**, 16099.

13 M. Mączka, M. Ptak, A. Gągor, D. Stefańska, J. K. Zaręba and A. Sieradzki, Methylhydrazinium Lead Bromide: Noncentrosymmetric Three-Dimensional Perovskite with Exceptionally Large Framework Distortion and Green Photoluminescence, *Chem. Mater.*, 2020, **32**(4), 1667–1673.

14 M. Mączka, A. Gagor, J. K. Zaręba, D. Stefanska, M. Drozd, S. Balciunas, M. Šimėnas, J. Banys and A. Sieradzki, Three-Dimensional Perovskite Methylhydrazinium Lead Chloride with Two Polar Phases and Unusual Second-Harmonic Generation Bistability above Room Temperature, *Chem. Mater.*, 2020, **32**(9), 4072–4082.

15 R. P. Hanna, I. K. Olesia, S. Sergiu and A. G. Il'ya, Aziridinium Cation Templating 3D Lead Halide Hybrid Perovskites, *Chem. Commun.*, 2022, **58**, 5745–5748.

16 W. J. Xu, P. F. Li, Y. Y. Tang, W. X. Zhang, R. G. Xiong and X. M. Chen, A Molecular Perovskite with Switchable Coordination Bonds for High-Temperature Multiaxial Ferroelectrics, *J. Am. Chem. Soc.*, 2017, **139**, 6369–6375.

17 B. Y. Wang, C. T. He, B. Huang, W. J. Xu, W. Xue, Z. Y. Du, W. X. Zhang and X. M. Chen, Thermal-Induced Reversible Ferroelastic Phase Transition in a New Bromethyl-Substituted Molecular Rotor, *Sci. China: Chem.*, 2015, **58**, 1137–1143.

18 G. J. Yuan, D. S. Shao, Z. Y. Yao, W. L. Liu and X. M. Ren, An Organometallic Half-Sandwich Supramolecular Complex {K(18-crown-6)(η^n-$C_6H_5B(C_6H_5)_3$)} (n = 1–6) Exhibiting a Reversible Breaking-Symmetry Phase

Transition and Switchable Dielectric Behavior, *Dalton Trans.*, 2018, **47**, 16835–16839.

19 G. J. Yuan, D. S. Shao, B. W. Hu, W. L. Liu and X. M. Ren, A Rotorlike Supramolecular Assembly, {[K(18-crown-6)] PbI_3}$_\infty$, with a Reversible Breaking–Symmetry Phase Transition near Room Temperature, *Inorg. Chem.*, 2020, **59**, 980–983.

20 C. Xue, S. Wang, W. L. Liu and X. M. Ren, Two-Step Structure Phase Transition, Dielectric Anomalies and Thermochromic Luminescence Behavior in a Direct Bandgap 2D Corrugated Layer Lead Chloride Hybrid of $[(CH_3)_4N]_4Pb_3Cl_{10}$, *Chem. – Eur. J.*, 2019, **25**, 5280–5287.

21 M. Mączka, J. K. Zaręba, A. Gągor, D. Stefańska, M. Ptak, K. Roleder, D. Kajewski, A. Soszyński, K. Fedoruk and A. Sieradzki, $[Methylhydrazinium]_2PbBr_4$, A Ferroelectric Hybrid Organic–Inorganic Perovskite with Multiple Nonlinear Optical Outputs, *Chem. Mater.*, 2021, **33**, 2331–2342.

22 X. Q. Huang, H. Yu, Z. K. Xu, T. Gan and Z. X. Wang, Tuning Dielectric Transitions in Two-Dimensional Organic–Inorganic Hybrid Lead Halide Perovskites, *Inorg. Chem.*, 2021, **60**, 16871–16877.

23 F. F. Wang, L. Huber, S. F. Maehrlein and X. Y. Zhu, Optical Anisotropy and Phase Transitions in Lead Halide Perovskites, *J. Phys. Chem. Lett.*, 2021, **12**, 5016–5022.

24 K. Xu, L. He, Y. Z. Wang, X. Meng, P. P. Shi and Q. Ye, $(C_7H_{18}N_2)PbI_4$: A 2D Hybrid Perovskite Solid-State Phase Transition Material with Semiconducting Properties, *Inorg. Chem.*, 2021, **60**, 10642–10647.

25 M. Bari, A. A. Bokov and Z. G. Ye, Ferroelastic Domains and Phase Transitions in Organic–Inorganic Hybrid Perovskite $CH_3NH_3PbBr_3$, *J. Mater. Chem. C*, 2021, **9**, 3096–3107.

26 D. Drozdowski, A. Gągor, D. Stefańska, J. K. Zaręba, K. Fedoruk, M. Mączka and A. Sieradzki, Three-Dimensional Methylhydrazinium Lead Halide Perovskites: Structural Changes and Effects on Dielectric, Linear, and Nonlinear Optical Properties Entailed by the Halide Tuning, *J. Phys. Chem. C*, 2022, **126**, 1600–1610.

27 X. N. Hua, W. Q. Liao, Y. Y. Tang, P. F. Li, P. P. Shi, D. W. Zhao and R. G. Xiong, A Room-Temperature Hybrid Lead Iodide Perovskite Ferroelectric, *J. Am. Chem. Soc.*, 2018, **140**, 12296–12302.

28 S. M. Liu, L. He, Y. Z. Wang, P. P. Shi and Q. Ye, Tunable Phase Transition, Band Gap and SHG Properties by Halogen Replacement of Hybrid Perovskites [(Thiomorpholinium)PbX_3, X = Cl, Br, I], *Chin. Chem. Lett.*, 2022, **33**, 1032–1036.

29 A. Sadhanala, S. Ahmad, B. Zhao, N. Giesbrecht, P. M. Pearce, F. Deschler, R. L. Z. Hoye, K. C. Godel, T. Bein, P. Docampo, S. E. Dutton, M. F. L. De Volder and R. H. Friend, Blue-Green Color Tunable Solution Processable Organolead Chloride-Bromide Mixed Halide Perovskites for Optoelectronic Applications, *Nano Lett.*, 2015, **15**, 6095–6101.

30 G. E. Eperon, S. D. Stranks, C. Menelaou, M. B. Johnston, L. M. Herz and H. J. Snaith, Formamidinium Lead Trihalide: a Broadly Tunable Perovskite for Efficient Planar Heterojunction Solar Cells, *Energy Environ. Sci.*, 2014, **7**, 982–988.

31 A. Sadhanala, F. Deschler, T. H. Thomas, S. E. Dutton, K. C. Goedel, F. C. Hanusch, M. L. Lai, U. Steiner, T. Bein, P. Docampo, D. Cahen and R. H. Friend, Preparation of Single-Phase Films of $CH_3NH_3Pb(I_{1-x}Br_x)_3$ with Sharp Optical Band Edges, *J. Phys. Chem. Lett.*, 2014, **5**, 2501–2505.

32 M. J. Wang, X. R. Chen, Y. B. Tong, G. J. Yuan, X. M. Ren and J. L. Liu, Phase Transition, Dielectrics, Single-Ion Conductance, and Thermochromic Luminescence of a Inorganic–Organic Hybrid of [Triethylpropylammonium]-[PbI_3], *Inorg. Chem.*, 2017, **56**, 9525–9534.

33 J. Y. Tian, D. B. Cordes, A. M. Z. Slawin, E. Zysman-Colman and F. D. Morrison, Progressive Polytypism and Bandgap Tuning in Azetidinium Lead Halide Perovskites, *Inorg. Chem.*, 2021, **60**, 12247–12254.

34 N. W. Thomas, Crystal Structure-Physical Property Relationships in Perovskites, *Acta Crystallogr., Sect. B: Struct. Sci.*, 1989, **45**, 337–344.

35 J. A. Alonso, M. J. Martinez-Lope, M. T. Casais and M. T. Fernandez-Diaz, Evolution of the Jahn–Teller Distortion of MnO6 Octahedra in $RMnO_3$ Perovskites (R = Pr, Nd, Dy, Tb, Ho, Er, Y): A Neutron Diffraction Study, *Inorg. Chem.*, 2000, **39**, 917–923.

36 M. W. Lufaso and P. M. Woodward, Jahn-Teller Distortions, Cation Ordering and Octahedral Tilting in Perovskites, *Acta Crystallogr., Sect. B: Struct. Sci.*, 2004, **60**, 10–20.

37 A. Basile, M. Hilder, F. Makhlooghiazad, C. Pozo-Gonzalo, D. R. MacFarlane, P. C. Howlett and M. Forsyth, Ionic Liquids and Organic Ionic Plastic Crystals: Advanced Electrolytes for Safer High Performance Sodium Energy Storage Technologies, *Adv. Energy Mater.*, 2018, **8**, 1703491.

38 A. Pinkert, K. N. Marsh, S. Pang and M. P. Staiger, Ionic Liquids and Their Interaction with Cellulose, *Chem. Rev.*, 2009, **109**, 6712–6728.

39 J. M. Bermúdez-García, M. Sánchez-Andújar, S. Castro-García, J. López-Beceiro, R. Artiaga and M. A. Señarís-Rodríguez, Giant Barocaloric Effect in the Ferroic Organic–Inorganic Hybrid [TPrA][$Mn(dca)_3$] Perovskite Under Easily Accessible Pressures, *Nat. Commun.*, 2017, **8**, 15715.

40 M. Mączka, A. Gągor, M. Ptak, D. Stefańska, L. Macalik, A. Pikul and A. Sieradzki, Structural, Phonon, Magnetic and Optical Properties of Novel Perovskite-Like Frameworks of TriBuMe[$M(dca)_3$] (TriBuMe = tributyl-methylammonium; dca = dicyanamide; M = Mn^{2+}, Fe^{2+}, Co^{2+}, Ni^{2+}), *Dalton Trans.*, 2019, **48**, 13006–13016.

41 Q. Kang, Y. Li, Z. Zhuang, D. Wang, C. Zhi, P. Jiang and X. Huang, Dielectric Polymer Based Electrolytes for High-Performance All-Solid-State Lithium Metal Batteries, *J. Energy Chem.*, 2022, **69**, 194–204.

42 N. Kara, A. Kiraci and H. Yurtseven, Calculation of the Spin-Lattice Relaxation Time and the Activation Energy Near the IV–III Phase Transition in Pyridinium

Fluorosulfonate $(C_5NH_6)FSO_3$, *Ferroelectrics*, 2022, **589**, 45–54.

43 Y. Qian, Y. M. Wang, L. Xu, W. W. Yao, D. S. Shao and X. M. Ren, Formation of Organic Ion Cocrystals, Phase Transition and Ion Conduction, *CrystEngComm*, 2022, **24**, 3962–3971.

44 J. Tauc, R. Grigorovici and A. Vancu, Optical Properties and Electronic Structure of Amorphous Germanium, *Phys. Status Solidi*, 1966, **15**, 627–637.

45 G. Kortem, W. Braun and G. Herzog, Principles and Techniques of Diffuse-Reflectance Spectroscopy, *Angew. Chem., Int. Ed. Engl.*, 1963, **2**, 333–341.

46 M. Parrinello, A. Rahman and P. Vashishta, Structural Transitions in Superionic Conductors, *Phys. Rev. Lett.*, 1983, **50**, 1073–1076.

47 J. Boyce and B. Huberman, Superionic Conductors: Transitions, Structures, Dynamics, *Phys. Rep.*, 1979, **51**, 189–265.

48 C. Xiao, J. Xu, K. Li, J. Feng, J. Yang and Y. Xie, Superionic Phase Transition in Silver Chalcogenide Nanocrystals Realizing Optimized Thermoelectric Performance, *J. Am. Chem. Soc.*, 2012, **134**, 4287–4293.

49 Y. Qian, D. S. Shao, W. W. Yao, N. Wan, X. Z. Wang and X. M. Ren, Ion Conduction and Complicated Phase Transition Behaviors in an Organic Ion Plastic Crystal, [Tetra-nbutylammonium]$_2$[Ni(maleonitriledithiolate)$_2$], *J. Phys. Chem. C*, 2020, **124**, 20722–20729.

50 Y. Qian, D. S. Shao, W. W. Yao, Z. Y. Yao, L. Wang, W. L. Liu and X. M. Ren, A Promising Phase Change Material with Record High Ionic Conductivity over a Wide Temperature Range of a Plastic Crystal Phase and Magnetic Thermal Memory Effect, *ACS Appl. Mater. Interfaces*, 2020, **12**, 28129–28138.

51 Y. Qian, J. Zhang, Y. M. Wang, W. W. Yao, D. S. Shao and X. M. Ren, Magnetic Bistable Organic Ionic Plastic Crystal with Room Temperature Ion Conductivity Comparable to NASICON and Superionic Conduction in a Broad Temperature Window, *Mater. Chem. Front.*, 2022, **6**, 793–801.

52 X. M. Ren, Q. J. Meng, Y. Song, C. S. Lu and C. J. Hu, Unusual Magnetic Properties of One-Dimensional Molecule-Based Magnets Associated with a Structural Phase Transition, *Inorg. Chem.*, 2002, **41**, 5686–5692.

53 Bruker APEX 2, *SAINT, XPREP*, Bruker AXS Inc., Madison, Wisconsin, USA, 2007.

54 Bruker SADABS, Bruker AXS Inc., Madison, Wisconsin, USA, 2001.

55 G. M. Sheldrick, *SHELXS-2014, Program for the Solution and Refinement of Crystal Structures*, University of Göttingen, Göttingen, Germany, 2014.

Dear Author

Please use this PDF proof to check the layout of your article. If you would like any changes to be made to the layout, you can leave instructions in the online proofing interface. First, return to the online proofing interface by clicking "Edit" at the top of the page, then insert a Comment in the relevant location. Making your changes directly in the online proofing interface is the quickest, easiest way to correct and submit your proof.

Please note that changes made to the article in the online proofing interface will be added to the article before publication, but are not reflected in this PDF proof.